materials

MDPI

Article

Low-Temperature Fabrication of Plate-like α-Al_2O_3 with Less NH_4F Additive

Haiyang Chen [1], Bin Li [1,*], Meng Liu [1], Xue Yang [2], Jie Liu [1], Tingwei Qin [1], Zejian Xue [1], Yun Xing [1] and Junhong Chen [1,*]

[1] School of Materials Science and Engineering, University of Science and Technology Beijing, Beijing 100083, China; chenhaiyang_123@163.com (H.C.); 17801052278@126.com (M.L.); liujie9697@163.com (J.L.); 18511074792@163.com (T.Q.); xue1998829@outlook.com (Z.X.); xingzhyun@163.com (Y.X.)

[2] School of Civil and Engineering, Hebei University of Architecture, Zhangjiakou 075000, China; yangxue19930817@163.com

* Correspondence: libin@ustb.edu.cn (B.L.); cjh2666@126.com (J.C.)

Abstract: Fluorinated compounds are effective mineralization agents for the fabrication of plate-like α-Al_2O_3. However, in the preparation of plate-like α-Al_2O_3, it is still an extremely challenging task to reduce the content of fluoride while ensuring a low synthesis temperature. Herein, oxalic acid and NH_4F are proposed for the first time as additives in the preparation of plate-like α-Al_2O_3. The results showed that plate-like α-Al_2O_3 can be synthesized at a low temperature of 850 °C with the synergistic effect of oxalic acid and 1 wt.% NH_4F. Additionally, the synergistic effect of oxalic acid and NH_4F not only can reduce the conversion temperature of α-Al_2O_3 but also can change the phase transition sequence.

Keywords: plate-like α-Al_2O_3; low temperature; oxalic acid; NH_4F; synergistic effect

check for updates

Citation: Chen, H.; Li, B.; Liu, M.; Yang, X.; Liu, J.; Qin, T.; Xue, Z.; Xing, Y.; Chen, J. Low-Temperature Fabrication of Plate-like α-Al_2O_3 with Less NH_4F Additive. *Materials* **2023**, *16*, 4415. https://doi.org/10.3390/ma16124415

Academic Editors: Andrea Di Schino and Wiesław Stręk

Received: 24 April 2023
Revised: 26 May 2023
Accepted: 14 June 2023
Published: 15 June 2023

1. Introduction

Alumina (Al_2O_3) is a prospective material due to its competitive thermochemical and mechanical features [1–4]. Among the dozen crystal structures in which Al_2O_3 exists, α-Al_2O_3 is the most thermodynamically stable phase, while the others are metastable transition phases [5]. Since α-Al_2O_3 is the only thermodynamically stable phase, the preparation of α-Al_2O_3 powders with various morphologies, including spherical, plates and fibers, has been sought by many scholars [1,6–9]. Among these morphologies, the plate-like α-Al_2O_3 powder can be applied as a filler for the thermal conductivity improvement of plastics, as a reinforcement for ceramic materials, and as an abrasive for polishing [10–15].

Until now, many strategies have been attempted to synthesize plate-like α-Al_2O_3, such as hydrothermal methods, melt salt methods, and chemical vapor deposition [13,16–18]. Regardless of the methods used, calcination is a necessary step for the fabrication of plate-like α-Al_2O_3. Since the phase transition from transitional alumina to α-Al_2O_3 involves drastic bond breaking and remaking, the thermal process usually requires temperatures greater than 1200 °C [19]. These temperatures not only impose higher requirements for the preparation equipment of α-Al_2O_3, but they also cause substantial mass transfer, leading to rapid growth of α-Al_2O_3 particle size [20]. Worse, when the sintering temperature exceeds the critical value, plate-like α-Al_2O_3 perhaps converts into particle-like grains [8]. Therefore, it is critical to reduce the synthesis temperature of α-Al_2O_3.

It is well known that fluorine-containing compounds can significantly reduce the synthesis temperature of α-Al_2O_3, and they are also considered effective mineralization agents for the fabrication of plate-like α-Al_2O_3 [5,7,8,14,21–31]. Hence, coupled with the low cost and simple process of α-Al_2O_3, the addition of fluorine-containing mineralization agents to alumina precursors has been used by many researchers for the preparation of

plate-like α-Al_2O_3. For example, Tian et al. [8] synthesized highly pure plate-like α-Al_2O_3 from a boehmite precursor with 5 wt.% NH_4F. Similarly, Wang et al. [21] also successfully prepared plate-like α-Al_2O_3 by thermal decomposition of ammonium aluminum carbonate hydroxide (AACH) adding 5 wt.% AlF_3. They thought that the formation of the intermediate compound AlOF accelerated the mass transfer of Al^{3+} and improved the growth rate along the crystal orientation of <10$\bar{1}$0>. Nevertheless, a shortcoming of these studies was the excessive use of F content, even as high as 20 wt.% in some cases [31]. When the concentration of F is excessive, both gaseous and particulate fluoride is toxic to plants and animals, and a series of diseases, such as fluorosis of bone and cancer, can be caused [24,32]. In this context, an extremely challenging objective is finding an effective strategy to not only reduce the concentration of F but also to maintain a low synthesis temperature in the process of preparing α-Al_2O_3 with fluoride as an additive. Currently, increasing interest has been focused on this aspect, but the existing research has been mostly theoretical, with almost no experimental research.

In our previous report [33], oxalic acid was confirmed to be helpful in reducing the resultant temperature of α-Al_2O_3 by 100 °C. Therefore, in this paper, we proposed for the first time adding oxalic acid and NH_4F as additives in the preparation process of plate-like α-Al_2O_3. The synergistic influences of oxalic acid and NH_4F on the crystal transition order of $Al(OH)_3$ were studied, and the optimum F content was explored. Simultaneously, the action mechanism of oxalic acid and NH_4F during the transformation was clarified based on the experimental results.

2. Experimental Procedures

The preparation process mainly involved the following starting materials: analytically pure $Al(OH)_3$ (>99.8%), analytically pure oxalic acid (>99.0%), analytically pure ammonium fluoride (NH_4F, >98.0%), and deionized water. Except for deionized water, which was home made in the laboratory, other raw materials were obtained from Sinopharm Chemical Reagent Co., Ltd., Shanghai, China. All raw materials were directly adopted without any further purification.

As in our previous work [33], first, oxalic acid solution with a concentration of 0.16 mol/L was prepared. Subsequently, 20 g of $Al(OH)_3$ and 60 mL of oxalic acid solution were mixed and ball-milled for 11 h. Then, 0, 0.25, 0.5, 1, and 2 wt.% NH_4F by weight of $Al(OH)_3$ was added to continue the ball milling for 1 h. Afterward, the resulting mixtures were air dried at 50 °C for 72 h. The obtained samples were labeled A1 (0 wt.%), A2 (0.25 wt.%), A3(0.5 wt.%), A4 (1 wt.%), and A5(2 wt.%), according to the amount of NH_4F. Finally, specimens A1–A5 were heated from room temperature to distinct temperatures (700, 750, 800, 850, 900, and 950 °C) at a heating rate of 5 °C/min holding for 3 h.

Phase composition analysis was performed with a D/max2500 X-ray diffractometer (Rigaku Industrial Corporation, Tokyo, Japan) using Cu Kα radiation (40 kV, 40 mA) at 2θ angles of 10–90°. Fourier transform infrared (FTIR) spectroscopy (Nicolet 380) was characterized using a spectrograph (Thermo Electron, Houston, TX, USA). A Nova Nano 450 scanning electron microscope (SEM, FEI Company, Hillsboro, OR, USA) was used to examine the microscopic morphologies of all specimens. X-ray photoelectron spectroscopy (XPS) was performed using an Escalab 50XI photoelectron spectrometer (VG Scientific Ltd., St Leonards, UK). Particle size distribution was collected by a Malvin laser particle size analyzer (Mastersizer 3000, Marvin Pan-alytical, Almelo, The Netherlands). Thermal gravimetry and differential scanning calorimetry (TG-DSC) curves were collected using a simultaneous TG-DTA/DSC apparatus (STA2500, NETZSCH-Gerätebau GmbH, Free State of Bavaria, Germany) under an ambient atmosphere with a heating rate of 10 °C/min up to 1300 °C.

3. Results and Discussion

Since the analytic results of A1 were applied in our previous reports [33], only A2–A5 were analyzed in this paper. To characterize the compositions of A2–A5, the spectra of

A2–A5 were recorded using the FTIR technique, as shown in Figure 1. Figure 1a exhibits the FTIR spectra in the infrared region of 400–4000 cm^{-1}. It was clear that the absorption peaks exhibited by A2–A5 were greatly similar to those of A1 reported in our previous work [33]. The only difference was that, with the increase in NH_4F content, the absorption peak at around 3200 cm^{-1}, corresponding to the stretching vibrations of N-H bonds, began to gradually appear, especially for A5. Among these absorption bands presented by A2–A5, the absorption bands centered at 3621, 3526, 3456, and 3393 cm^{-1} can be assigned to the stretching vibrations of hydroxyl groups in $Al(OH)_3$ and adsorbed water [34]. The intensive bands shown at 1704, 1415, and 1297 cm^{-1} were related to the stretching vibration of carboxyl COO^-, implying that a surface complex ($Al_2C_2O_8H_4$), as we reported previously, had been formed due to the interaction of oxalic acid and $Al(OH)_3$ [33]. Regarding the bands in the 400 to 1200 cm^{-1} interval (local amplification in Figure 1b), the weak band observed at 915 cm^{-1} was caused by the deformation of surface hydroxyls. The vibration bands at 1022, 970, 803, 751, 666, 560, 517, 451, and 423 cm^{-1} were associated with the stretching and bending of Al-O bonds [35]. With the target of understanding the effects of F^- ion on the structure of $Al(OH)_3$, the changes in the spectra attributed to Al-O bonds between A2 and A5 were carefully observed. Interestingly, these vibration bands were identical in position and shape except for the intensity, revealing that F^- ions did not bond with Al^{3+} ions and O^{2-} ions on the surface of $Al(OH)_3$, perhaps because of the surface of $Al(OH)_3$ was covered with hydroxyl groups.

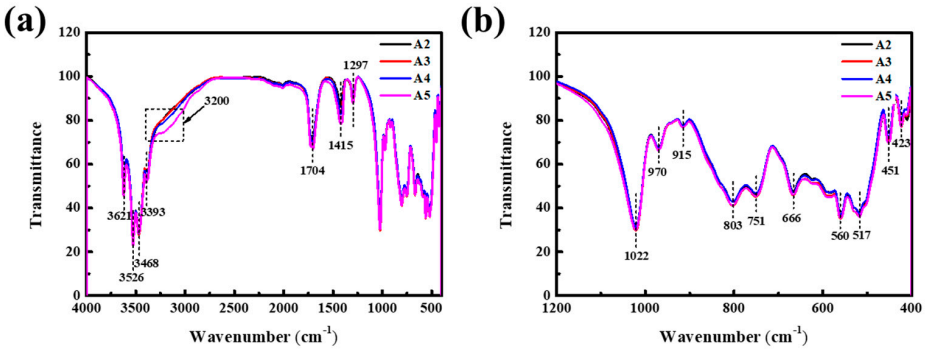

Figure 1. FTIR spectra of: (**a**) the specimens A2–A5; (**b**) local amplification at 1200–400 cm^{-1}.

The SEM pictures of A2–A5 are illustrated in Figure 2. As shown in Figure 2a, the microstructure of A2 mainly consisted of granular structures, in which a small number of sheets were found, as shown by the red arrow. The formation process of granular particles was discussed in our previous research [33]. As the content of NH_4F increased, the microstructures of A3-A5 exhibited little change compared with those of A2 (See Figure 2b–d). The illustration in Figure 2d perfectly presents the morphology of granular particles.

Figure 3a–d demonstrates the XRD patterns of A2–A5 thermally treated at different temperatures holding for 3 h. Learning from the literature, α-Al_2O_3 is usually obtained through a sequence of polymorphic transformations because Al_2O_3 exists in several different metastable phases. From Figure 3a, it can be clearly observed that, at 700 and 750 °C, the XRD pattern of A2 presented four peaks at $2\theta = 37.3°$, 42.8°, 46.3°, and 67.0°, corresponding to χ-Al_2O_3 and κ-Al_2O_3 [5]. For calcination at 800 °C, except for the peaks emerging at 700 °C, some shallow peaks at $2\theta = 25.6°$, 35.1°, 43.3°, and 57.5°, indexed as α-Al_2O_3, can be detected. As the temperature increased to 850 °C, instead of the peaks of χ-Al_2O_3, many characteristic peaks ascribed to κ-Al_2O_3 can be observed, and κ-Al_2O_3 became the major phase coexisting with α-Al_2O_3. With the further increase in calcination temperature, the peak intensity of κ-Al_2O_3 gradually decreased. At 950 °C, the peak of κ-Al_2O_3 disappeared, and the pattern only had the peak of α-Al_2O_3. From the above results, for sample A2, the phase transition process was: $Al(OH)_3 \rightarrow \chi$-$Al_2O_3 \rightarrow \kappa$-$Al_2O_3 \rightarrow \alpha$-$Al_2O_3$; and the synthetic temperature of α-Al_2O_3 was 950 °C, in agreement with our previous study [33]. Regarding A3-A5, the synthesis temperatures of α-Al_2O_3 were 900, 850, and 800 °C, re-

spectively, which were all lower than those of A1 and A2. In addition, with the growth of NH_4F content, χ- and κ-Al_2O_3 were replaced by γ- and θ-Al_2O_3 in the polycrystalline transformation of Al_2O_3, respectively. Surprisingly, except for γ-Al_2O_3, no trace of other transitional forms of Al_2O_3 were detected before α-Al_2O_3 was obtained for A5.

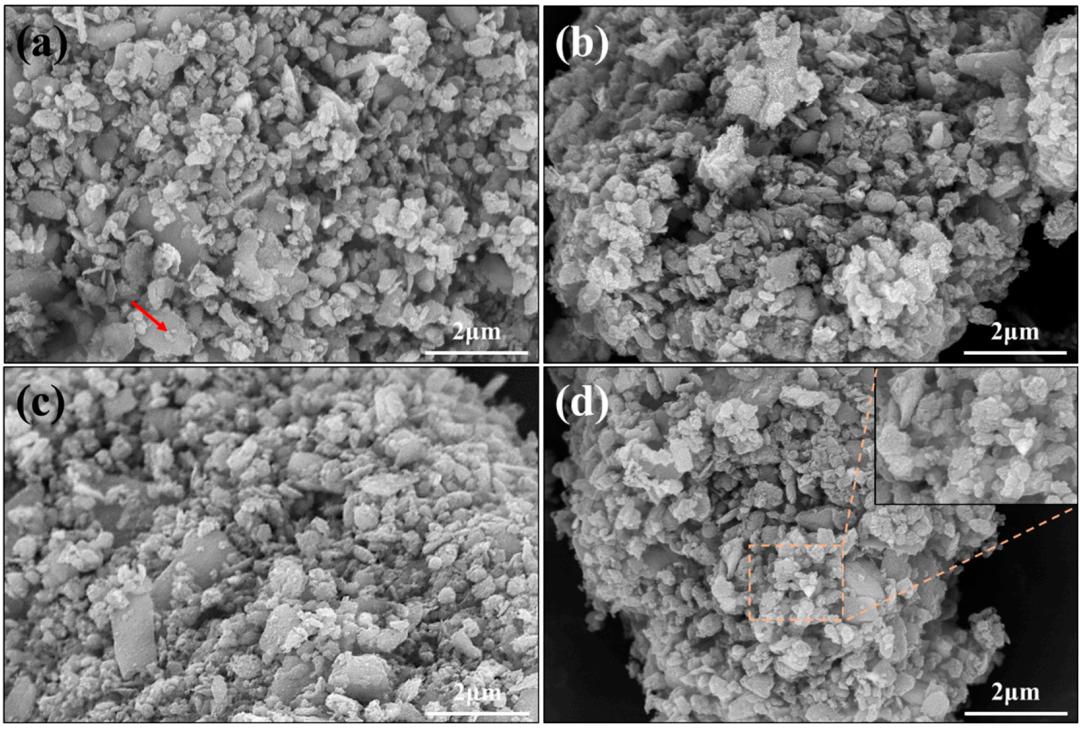

Figure 2. SEM pictures of A2–A5: (**a**) A2; (**b**) A3; (**c**) A4; (**d**) A5.

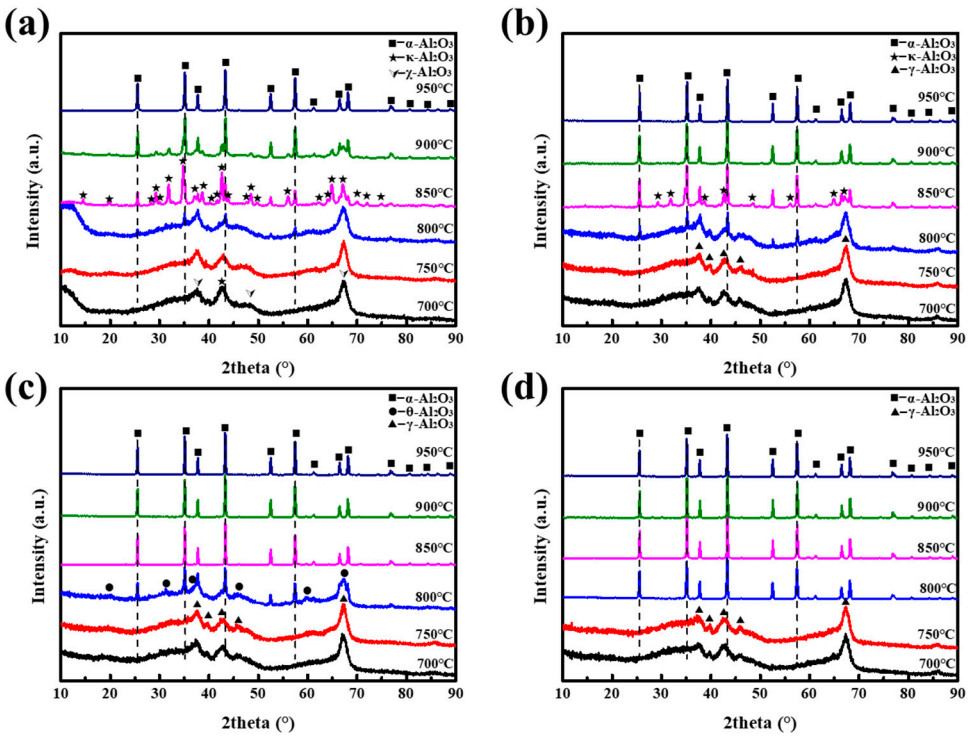

Figure 3. XRD patterns of the alumina phases received from A2–A5 at different calcination temperatures: (**a**) A2; (**b**) A3; (**c**) A4; (**d**) A5.

Aiming to further study the influences of oxalic acid and NH_4F on the transformation sequence of α-Al_2O_3, specimen A5 was fired at 800 °C with a heating rare 5 °C/min for different dwell times (10, 30, 60, and 120 min). The XRD images are illustrated in Figure 4. As shown in Figure 4a, the intense diffraction patterns attributed to θ-Al_2O_3 were observed for A5 thermally treated at 800 °C for 10 min, as well as some shallow patterns indexed as α-Al_2O_3. With the prolongation of calcination time, α-Al_2O_3 gradually became the main phase. Moreover, the grain size of as-received α-Al_2O_3 also displayed an upward trend according to the Scherrer formula, as illustrated in Figure 4b. By combining the results obtained from Figure 3c,d and Figure 4, the phase transformation sequence of A4 and A5 was $Al(OH)_3$ → γ-Al_2O_3 → θ-Al_2O_3 → α-Al_2O_3, which was different from that of A1 and A2.

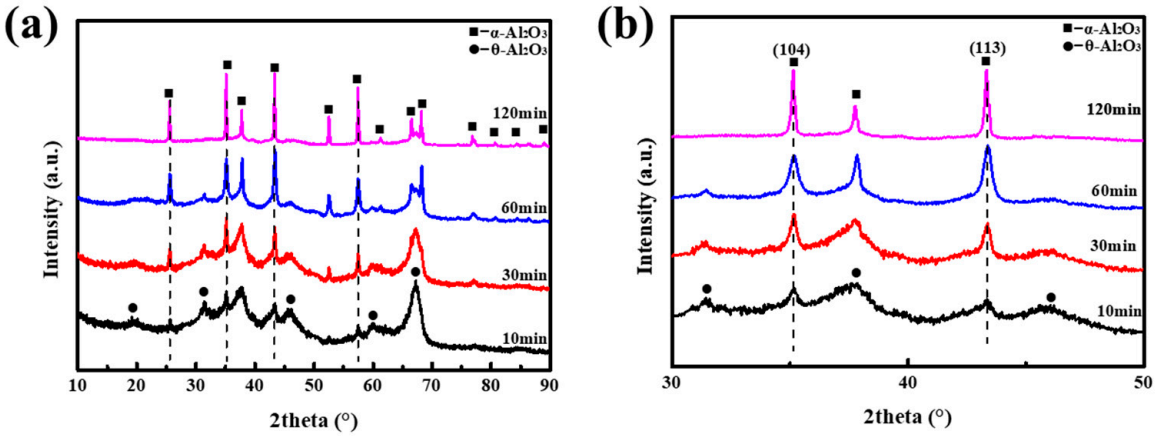

Figure 4. XRD patterns of: (**a**) the transition Al_2O_3 as obtained from A5 at 800 °C for distinct times; (**b**) local amplification at 2θ = 30°–50°.

S. J. Wilson [36] suggested that the difference in polycrystalline transition sequences was usually related to the difference in starting materials. In accordance with the results of FTIR, the crystal structure of $Al(OH)_3$ was not altered by the introduction of NH_4F. Therefore, it can be speculated that the structure of the reagent changed during the sintering process. After all, NH_4F had a low decomposition temperature, beyond which NH_4F decomposed into NH_3 and HF gas. The presence of HF gas perhaps plays a significant role in the structural changes of the sintered materials. Figure 5 demonstrates the high-resolution XPS spectra of the transitional Al_2O_3 received from A5 at a calcination temperature of 500 °C. Notably, in addition to the characteristic peaks of Al 2p, Al 2s, and O 1s as expected, an exclusive peak ascribed to F 1s can also be detected (Figure 5a). The O 1s region can be attributed to the contributions of the binding energy of O-Al at 530.8 eV and Al-O-H at 532.4 eV (Figure 5b). However, the binding energy of O-Al and Al-O-H exhibited here was higher than that reported in the other literature, which may be caused by the existence of F. With respect to Al 2p spectrum, two peaks centered at 74.2 eV and 75.6 eV, corresponding to the binding energy of Al-O and Al-F, respectively were observed (Figure 5c). Accordingly, the individual line presented one peak at 685.7 eV belonging to the binding energy of F-Al (Figure 5d). The results of XPS confirmed that F existed on the surface of the calcined materials. Adopting $Al(OH)_3$ as a starting material, the first metastable phase received was χ-Al_2O_3, which inherited the arrangement of oxygen anions in the crystal structure of $Al(OH)_3$, and Al^{3+} ions occupied the octahedral position in the hexagonal oxygen layer. In comparison, the stacking of χ-Al_2O_3 in the c direction demonstrated extremely obvious disorder [37,38]. Consequently, it turned out that $Al(OH)_3$ showed a significant disorder along the c axis during its dehydration, which may be an opportunity for gaseous HF to change the structure of the starting regent in calcination. The gaseous HF working with Al^{3+} ions on the surface of the precursor in calcination might cause the collapse of the dis-

ordered Al-O octahedron, resulting in the formation of γ-Al_2O_3 so that the polycrystalline transformation sequence changed to $Al(OH)_3 \rightarrow \gamma$-$Al_2O_3 \rightarrow \theta$-$Al_2O_3 \rightarrow \alpha$-$Al_2O_3$.

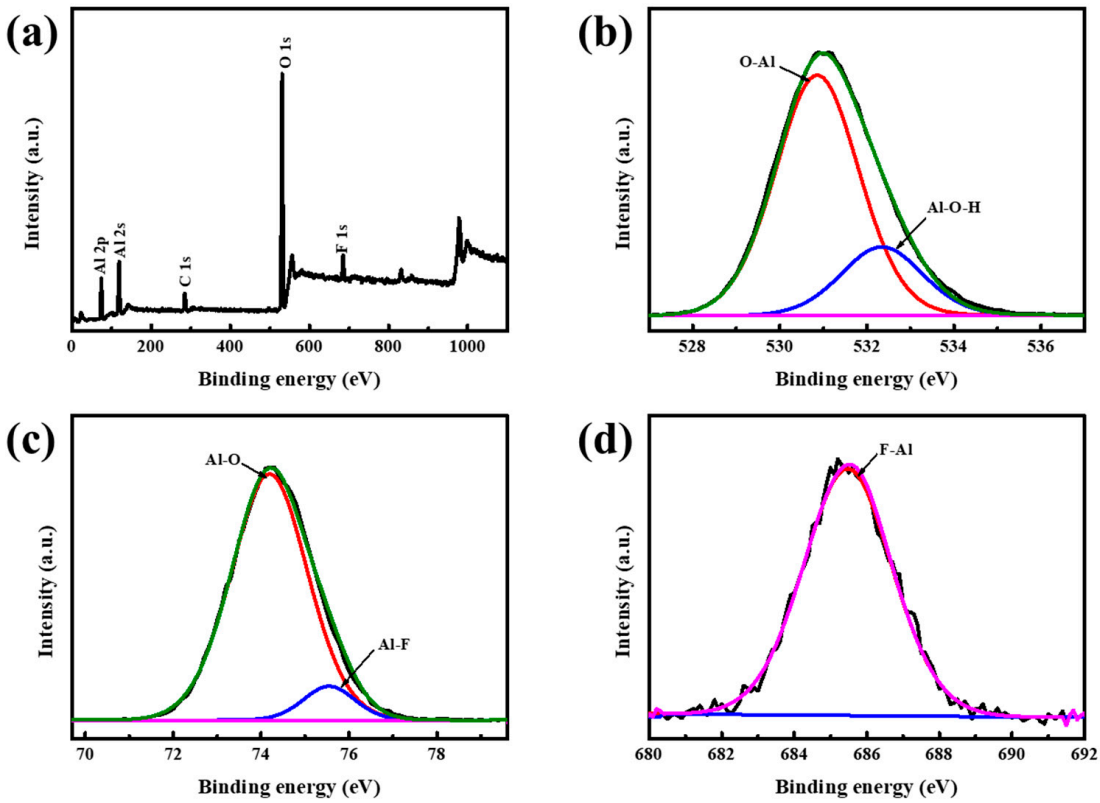

Figure 5. XPS spectrum of transition Al_2O_3 as-obtained from A5 at 500 °C (**a**); the overall XPS spectrum and the individual lines of: (**b**) O 1s; and (**c**) Al 2p (**d**) F 1s.

Figure 6 shows the TG-DSC curves of $Al(OH)_3$, A1, and A5. As presented in Figure 6a, the TG-DSC curves of $Al(OH)_3$ can be divided into two stages. The first stage, with a mass loss of 33.8% exhibited, two endothermic peaks at about 85 and 292 °C. These endothermic peaks were related to the evaporation of physically adsorbed water and the decomposition of $Al(OH)_3$. In the second stage, weight loss of around 2% can be observed, corresponding to the removal of hydroxyl groups from the transition Al_2O_3 surface. Furthermore, two exothermic peaks were displayed at 870 and 1120 °C, which were caused by the appearance of κ- and α-phases, respectively [39]. Similar to $Al(OH)_3$, the TG-DSC curves of A1 also included two steps, two endothermic peaks and two exothermic peaks, as shown in Figure 6b. The difference was that the two endothermic peaks were decreased to 800 and 1050 °C, respectively, and the heat release increased when the α-phase appeared. The growth in heat release indicated that the nucleation amount of α-Al_2O_3 increased. There were two main reasons for the decrease in the phase transition temperature and the increase in the nucleation number. One was that the complex generated by $Al(OH)_3$ and oxalic acid can act as seeds, providing low energy positions for heterogeneous nucleation. On the other hand, at greater than 400 °C, the number of transition Al_2O_3 surface hydroxyl groups obtained from A1 was approximately twice that of the transition Al_2O_3 obtained from $Al(OH)_3$, which can be obtained from the mass loss in the second stage of TG-DSC. Of course, this outcome also indicated that, at greater than 400 °C, A1 released twice as many water molecules as $Al(OH)_3$ released. As is known, the size of metastable Al_2O_3 must reach a critical crystal diameter before converting to α-Al_2O_3 [40]. The water vapor produced by dehydroxylation contributes to the coarsening of metastable Al2O3 to reach the critical crystal size [41]. Moreover, the formation of vacancies by dehydroxylation is also beneficial to the rearrangement of the Al_2O_3 lattice structure [42]. Therefore, A1 is

more easily converted into α-Al_2O_3 than $Al(OH)_3$. In contrast with $Al(OH)_3$ and A1, for the TG-DSC curves of A5, the exothermic peak attributed to α-Al_2O_3 nucleation that we cared about decreased to 940 °C and was more intense, related to the mass transfer of AlOF gas, as well as the reasons mentioned for A1. Additionally, C. Barth et al. [43] believed that, once α-Al_2O_3 at a high temperature was exposed to water, $Al(OH)_3$ microcrystalline clusters would form on the surface of α-Al_2O_3. In our work, the XPS of transition Al2O3 mentioned above confirmed the presence of Al-F bonds, which might produce AlF_3 clusters at the position of Al-F bonds, providing nucleation sites for α-Al_2O_3, which was also responsible for lowering the resultant temperature of α-Al_2O_3. In short, α-Al_2O_3 can be obtained at a low temperature under the synergistic effects of oxalic acid and NH_4F. Nevertheless, the synthesis temperature of α-Al_2O_3 obtained by the results of TG-DSC was higher than that shown by XRD, which may be caused by the high heating rate and purging of air during the operation process of TG-DSC.

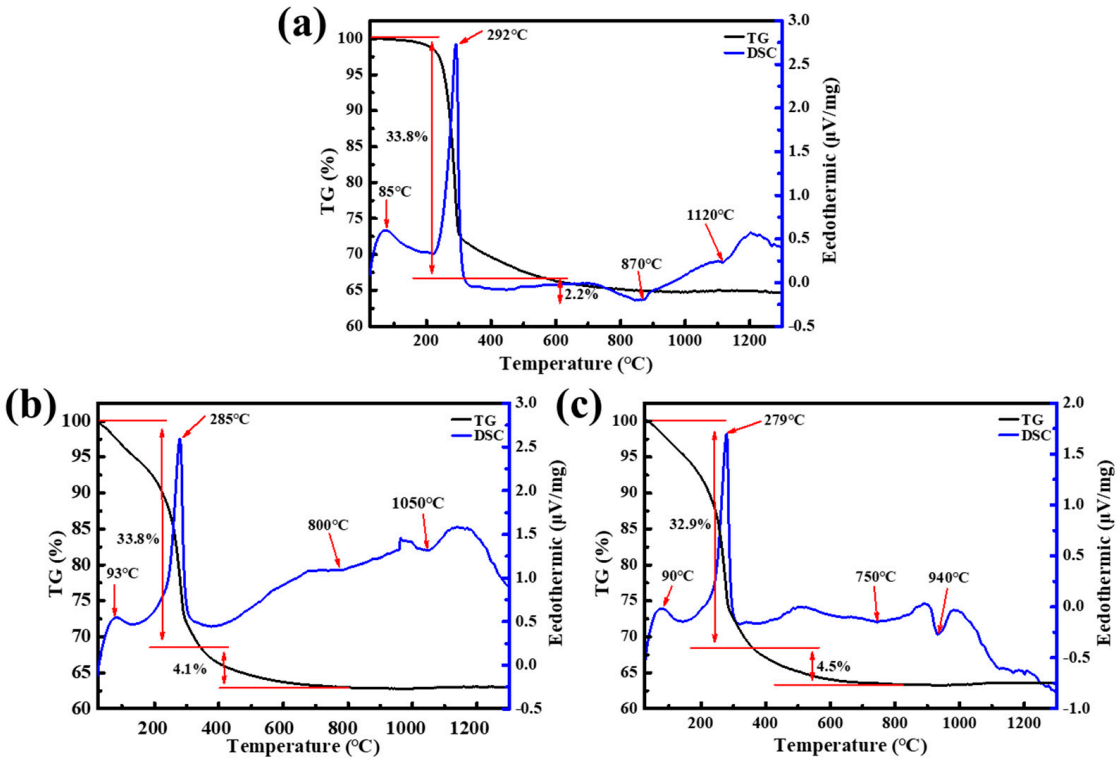

Figure 6. TG-DSC curves of: (**a**) $Al(OH)_3$; (**b**) A1; (**c**) A5.

Figure 7 shows SEM images of α-Al_2O_3 obtained from A2–A5 at different sintering temperatures. As can be seen from Figure 7a, the produced α-Al_2O_3 of A2 at 950 °C displayed a granular microstructure. Different from A2, at the same temperature, a drum-like architecture of α-Al_2O_3 particles was obtained for A3, while the α-Al_2O_3 prepared by A4 and A5 presented a plate-like structure, as illustrated in Figure 6b,c. Meanwhile, by carefully comparing the obtained α-Al_2O_3 in Figure 6b,c, it can be seen that the particle diameter of α-Al_2O_3 gradually increased with the increase in NH_4F content, while the thickness exhibited a decreasing trend. From the perspective of crystal growth, the microstructure of materials depends on the growth rate of the crystal plane. The remaining crystal surface is a plane with a slow growth rate. The inset in Figure 6b perfectly exhibits the crystal plane of α-Al_2O_3 obtained from A3 at 950 °C. According to a study [44], the side of the drum-shaped α-Al_2O_3 corresponds to the crystal plane of (2243), and the front side belongs to the (0001) plane. Different from the side of drum-shaped α-Al_2O_3, the side of the plate-like structure synthesized from A4 and A5 was ascribed with an (1120) plane. It was reported that F^- ions can work with Al^{3+} ions and adsorb on the crystal face of α-Al_2O_3.

In α-Al_2O_3 unit cells, the (0001) plane has close-packed atoms, lending themselves to more bare Al^{3+} ions on this crystal face. As a result, F^- ions tended to adsorb on the (0001) plane, limiting the deposition of α-Al_2O_3 on this face and bringing down its growth rate, resulting in the retention of the (0001) plane [21]. Of course, this was also responsible for the larger size and thinner thickness of α-Al_2O_3 obtained in the case of higher NH_4F content. In general, a small primary grain size was helpful in improving the mechanical properties of ceramic bodies. Figure 7e,f illustrates the SEM images of α-Al_2O_3 synthesized at 850 °C from A4 and at 800 °C from A5. Apparently, the produced α-Al_2O_3 presented similar particle sizes. Considering the particle size of as-received α-Al_2O_3, the F content, and the resultant temperature, under the synergistic effects of oxalic acid and NH_4F, mixing 1 wt.% NH_4F was optimal. In summary, plate-like α-Al_2O_3 can be successfully synthesized by the incorporation of 1 wt.% NH_4F with the assistance of oxalic acid at 850 °C. Table 1 illustrates detailed information about the synthesis of α-Al_2O_3 when fluorine-containing mineralizing agents are used. Compared with other reports, the fluoride content and synthesis temperature in this study were the lowest when the morphology of as-synthesized α-Al_2O_3 was plate-like, confirming the validity of our work.

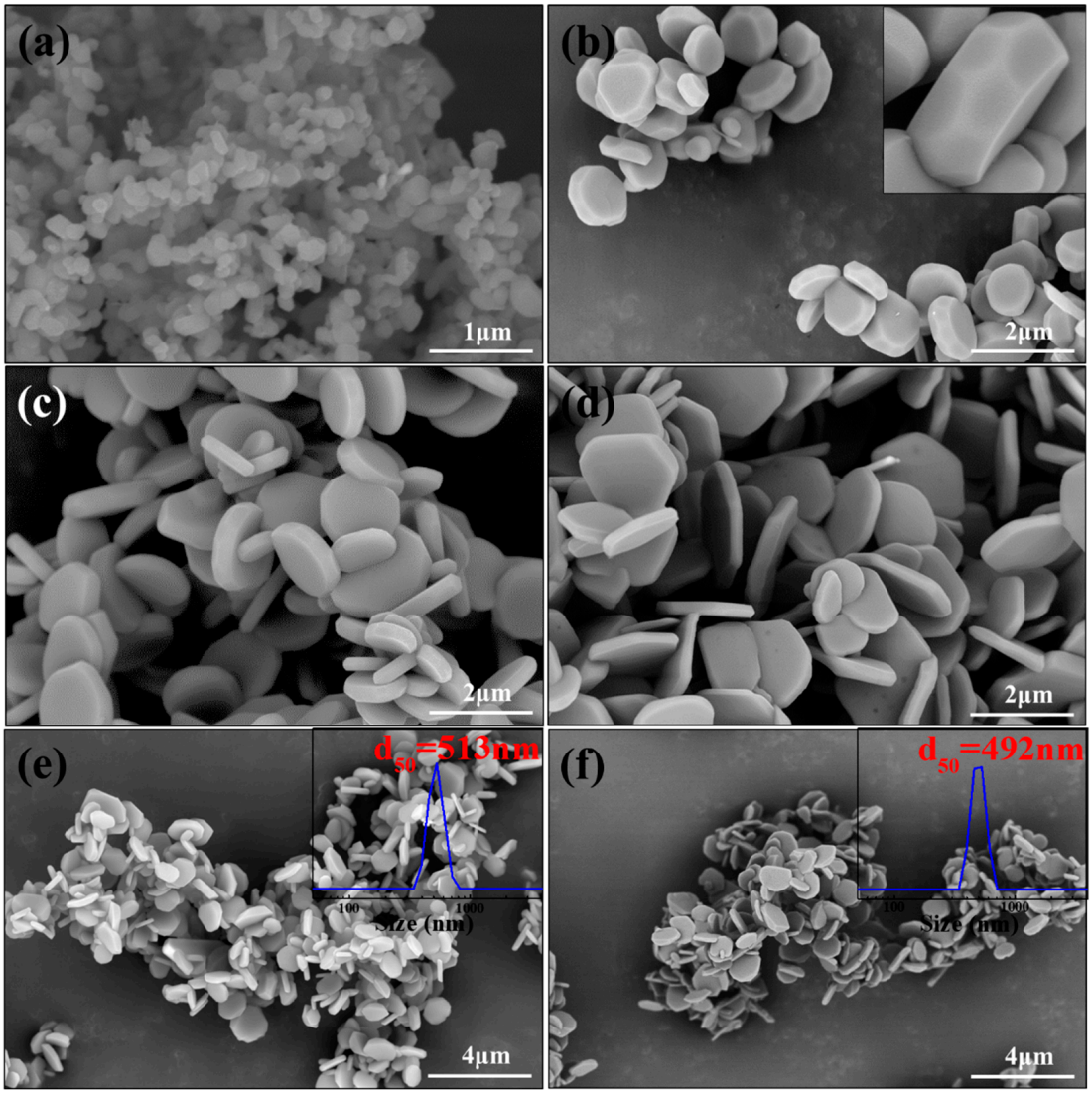

Figure 7. SEM images of α-Al_2O_3 obtained from A2–A5 at different temperatures: (**a**) A2-950; (**b**) A3-950; (**c**) A4-950; (**d**) A5-950; (**e**) A4-850; (**f**) A5-800.

Table 1. Detailed information about the synthesis of α-Al_2O_3 with fluoride as additives.

Morphology	Additive	Mixing Amount	Material	Temperature/Time	Ref.
Polyhedral	AlF_3	1 wt.%	$Al(OH)_3$	910 °C/3 h	[5]
Sphere-like	NH_4BF_4	5 wt.%	$Al(OH)_3$	1450 °C/3 h	[7]
Plate-like	NH_4F	5 wt.%	AlOOH	900 °C/2.5 h	[8]
Plate-like	NH_4F+NH_4F	5 wt.% + 5 wt.%	$Al(OH)_3$	1300 °C/3 h	[14]
Plate-like	AlF_3	5 wt.%	AACH	1200 °C/1 h	[21]
Plate-like	AlF_3	2 wt.%	AIP	900 °C/3 h	[22]
Plate-like	AlF_3 NH_4F	2.8 wt.% of F	AlOOH	1050 °C/1 h 950 °C/1 h	[23]
Plate-like	AlF_3	0.6 wt.%	t-$Al_2O_3Al(OH)_3$	1000 °C/0.5 h 950 °C/0.5 h	[24]
Plate-like	AlF_3	1 mol%	$Al(OH)_3$	750 °C/10 h	[25]
Plate-like	AlF_3	2 mol%	AlOOH	750 °C/10 h	[26]
Plate-like	ZnF_2 AlF_3	-	$Al(NO_3)_3$	920 °C/10 h 900 °C/1 h	[28]
Square-like	NH_4F	2 wt.%	γ-Al_2O_3	1300 °C/2 h	[30]
Plate-like	Oxalic acid + NH_4F	0.16 mol/L + 1 wt.%	$Al(OH)_3$	850 °C/3 h	This work

4. Conclusions

In the current work, oxalic acid and NH_4F were proposed for the first time as additives in the preparation of plate-like α-Al_2O_3. The results showed that plate-like α-Al_2O_3 can be synthesized at a low temperature of 850 °C with the synergistic effects of oxalic acid and 1 wt.% NH_4F. Both the synthesis temperature and the content of fluoride were lower than in other reports. With the increase in NH_4F content, due to the adsorption of F^- and the formation of AlOF gas, the morphology of the as-obtained α-Al_2O_3 changed from granular to plate-like, and the resultant temperature presented a downward trend. Additionally, owning to the adsorption of HF on the starting materials in sintering, the transition order of α-Al_2O_3 was changed from $Al(OH)_3 \rightarrow \chi$-$Al_2O_3 \rightarrow \kappa$-$Al_2O_3 \rightarrow \alpha$-$Al_2O_3$ to $Al(OH)_3 \rightarrow \gamma$-$Al_2O_3 \rightarrow \theta$-$Al_2O_3 \rightarrow \alpha$-$Al_2O_3$.

Author Contributions: Conceptualization, H.C., B.L. and J.C.; Methodology, H.C. and J.C.; Software, H.C. and M.L.; Formal analysis, H.C.; Investigation, J.L., T.Q., Z.X. and Y.X.; Resources, H.C.; Writing—original draft, H.C. and X.Y.; Supervision, B.L., M.L., X.Y. and J.C.; Funding acquisition, B.L. and J.C. All authors have read and agreed to the published version of the manuscript.

Funding: This research was funded by the National Nature Science Foundation of China (No. 51874027) and Fundamental Research Funds for the Central Universities (No. FRF-TP-19-003A1).

Institutional Review Board Statement: Not applicable.

Informed Consent Statement: Not applicable.

Data Availability Statement: No new data were created or analyzed in this study. Data sharing is not applicable to this article.

Acknowledgments: The authors express their appreciation to the National Nature Science Foundation of China (No. 51874027) and Fundamental Research Funds for the Central Universities (No. FRF-TP-19-003A1).

Conflicts of Interest: The authors declare no conflict of interest.

References

1. Wang, Z.; Mai, Z.; Wu, Y.; Wang, Y.; Cao, Z.; Li, M.; Fan, B.; Shao, G.; Wang, H.; Xu, H.; et al. Preparation of spherical α-Al_2O_3 nanoparticles by microwave hydrothermal synthesis and addition of nano-Al seeds. *J. Am. Ceram. Soc.* **2022**, *105*, 5585–5597.
2. Panasyuk, G.P.; Belan, V.N.; Voroshilov, I.L.; Kozerozhets, V.I.; Luchkov, V.; Kondakov, D.F.; Demina, L.I. The study of hydrargillite and γ-alumina conversion process in boehmite in different hydrothermal media. *Theor. Found. Chem. Eng.* **2013**, *47*, 415–421.

3. Xu, X.; Zhou, S.; Wu, J.; Zhang, Q.; Zhang, Y.; Zhu, G. Preparation of highly dispersive solid microspherical α-Al_2O_3 powder with a hydrophobic surface for stereolithography-based 3D printing technology. *Ceram. Int.* **2020**, *46*, 1895–1906.
4. Kozerozhets, I.V.; Panasyuk, G.P.; Semenov, E.A.; Danchevskaya, M.N.; Azarova, L.A.; Simonenko, N.P. Transformations of nanosized boehmite and γ-Al_2O_3 upon heat treatment. *Russ. J. Inorg. Chem.* **2020**, *65*, 587–591.
5. Zhu, L.; Liu, L.; Sun, C.; Zhang, X.; Zhang, L.; Gao, Z.; Ye, G.; Li, H. Low temperature synthesis of polyhedral α-Al_2O_3 nanoparticles through two different modes of planetary ball milling. *Ceram. Int.* **2020**, *46*, 28414–28421.
6. Miyake, K.; Hirata, Y.; Shimonosono, T.; Sameshima, S. The Effect of particle shape on sintering behavior and compressive strength of porous alumina. *Materials* **2018**, *11*, 1137. [CrossRef]
7. Li, S.; Zhu, L.; Liu, L.; Chen, L.; Li, H.; Sun, C. Influence of high-energy ball milling and additives on the formation of sphere-like α-Al_2O_3 powder by high-temperature calcination. *Z. Naturforsch. B* **2018**, *73*, 589–596.
8. Tian, Q.; Zhang, Y.; Yang, X.; Dai, J.; Lv, Z. Influences of NH4F on transformation and morphology of high-pure α-alumina. Mater. *Res. Express* **2017**, *4*, 105904.
9. Li, X.; Su, X.; Xiao, H.; Chen, L.; Li, S.; Tang, M. Continuous α-Al_2O_3 fibers grown by seeding with in-situ suspension. *Ceram. Int.* **2020**, *46*, 15638–15645.
10. Hill, R.; Danzer, R.; Paine, R. Synthesis of aluminum oxide platelets. *J. Am. Ceram. Soc.* **2001**, *84*, 514–520.
11. Zhou, J.; Laoui, T.; Biest, O. Toughening of X-sialon with Al_2O_3 platelets. *J. Eur. Ceram. Soc.* **1995**, *15*, 297–305.
12. Karl-Heinz Heussner, N.C. Yttria- and ceria-stabilized tetragonal zirconia polycrystals (Y-TZP, Ce-TZP) reinforced with $A1_2O_3$ platelets. *J. Eur. Ceram. Soc.* **1989**, *5*, 193–200.
13. Jin, X.; Gao, L. Size control of α-$A1_2O_3$ platelets synthesized in molten Na_2SO_4 flux. *J. Am. Ceram. Soc.* **2004**, *87*, 533–540.
14. Liu, L.; Zhang, X.; Zhu, L.; Wei, Y.; Guo, C.; Li, H. Preparation of hexagonal micro-sized α-$A1_2O_3$ platelets from a milled $Al(OH)_3$ precursor with NH4F and NH4Cl additives. *Z. Naturforsch. B* **2019**, *74*, 579–583.
15. Yin, X.; Zhang, Q.; Liu, J.; Zhong, X.; Chai, C. Polishing property of α-Al_2O_3 nanoflakes prepared by self-burning method. *Acta Phys-Chim. Sin.* **2009**, *25*, 1443–1448.
16. Suchanek, W.; Garcés, J.; Fulvio, P.; Jaroniec, M. Hydrothermal synthesis and surface sharacteristics of novel alpha alumina nanosheets with controlled chemical composition. *Chem. Mater.* **2010**, *22*, 6564–6574.
17. Zhu, L.; Tu, R.; Huang, Q. Molten salt synthesis of α-Al_2O_3 platelets using $NaAlO_2$ as raw material. *Ceram. Int.* **2012**, *38*, 901–908.
18. Wei, M.; Zhi, D.; Choy, K. Novel synthesis of α-alumina hexagonal nanoplatelets using electrostatic spray assisted chemical vapour deposition. *Nanotechnology* **2006**, *17*, 181–184.
19. Amrute, A.; Lodziana, Z.; Schreyer, H.; Weidenthaler, C.; Schuth, F. High-surface-area corundum by mechanochemically induced phase transformation of boehmite. *Science* **2019**, *366*, 485–489.
20. Deng, B.; Advincula, P.; Luong, D.; Zhou, J.; Zhang, B.; Wang, Z.; McHugh, E.; Chen, J.; Carter, R.; Kittrell, C.; et al. High-surface-area corundum nanoparticles by resistive hotspot-induced phase transformation. *Nat. Commun.* **2022**, *13*, 5027.
21. Wang, W.; Bi, J.; Qi, Y.; Zhang, Z.; Xing, Z.; Zhu, H.; Guo, D.; Xu, J.; Bai, Y. Preparation of micrometer-sized α-Al_2O_3 platelets by thermal decomposition of AACH. *Powder Technol.* **2010**, *201*, 273–276.
22. Fu, G.; Wang, J.; Kang, J. Influence of AlF_3 and hydrothermal conditions on morphologies of α-Al_2O_3. T. *Nonferr. Metal. Soc.* **2008**, *18*, 743–748.
23. Tian, Q. The influences of fluorides on the transformation of α-alumina crystals. *Ceram.-Silik.* **2017**, *64*, 357–366.
24. Riello, D.; Zetterström, C.; Parr, C.; Braulio, M.; Moreira, M.; Gallo, J.; Pandolfelli, V. AlF_3 reaction mechanism and its influence on α-Al_2O_3 mineralization. *Ceram. Int.* **2016**, *42*, 9804–9814.
25. Kim, H.; Park, N.; Lee, T.; Kang, M. Effect of AlF3 seed concentrations and calcination temperatures on the crystal growth of hexagonally shaped α-alumina powders. *Ceram. Int.* **2014**, *40*, 3813–3818.
26. Kim, H.; Kang, M. Rapid crystal phase transformation into hexagonally shaped α-alumina using AlF_3 seeds. *J. Sol-Gel Sci. Techn.* **2013**, *68*, 110–120.
27. Shimbo, M.; Yamamoto, O.; Hayashi, S.; Nakagawa, Z. Influence of addition of AlF_3 on thermal decomposition of gibbsite and phase transition of the intermediate alumina to α-Al_2O_3. *J. Ceram. Soc. Jpn.* **2007**, *115*, 536–540.
28. Wu, Y.; Pezzotti, G.; Guo, J. Influence of AlF3 and ZnF2 on the phase transformation of gamma to alpha alumina. *Mater. Lett.* **2002**, *52*, 366–369.
29. Živkovic, Ž.; Štrbac, N.; Šesták, J. Influence of fluorides on polymorphous transformation of α-Al_2O_3 formation. *Thermochim. Acta* **1995**, *266*, 293–300.
30. Zhu, L.; Sun, C.; Chen, L.; Lu, X.; Li, S.; Ye, G.; Liu, L. Influences of NH4F additive and calcination time on the morphological evolution of α-Al2O3 from a milled γ-Al_2O_3 precursor. *Z. Naturforsch. B* **2017**, *72*, 665–670.
31. Kang, J.; Wang, J.; Zhang, W. Influence of AlF3 additive on microstructure of alumina powder. *Light Met.* **2008**, *3*, 13–16.
32. Islam, M.; Patel, R. Thermal activation of basic oxygen furnace slag and evaluation of its fluoride removal efficiency. *Chem. Eng. J.* **2011**, *169*, 68–77.
33. Chen, H.; Ren, B.; Chen, L.; Zhao, F.; Bai, Q.; Chen, J.; Li, B. Preparation of equiaxed α-Al_2O_3 by adding oxalic acid. *Ceram. Int.* **2021**, *47*, 31512–31517.
34. Ibrahim, D.; Abu-Ayana, Y. Preparation and characterization of ultrafine alumina via sol–gel polymeric route. *Mater. Chem. Phys.* **2008**, *111*, 326–330.

35. Meher, T.; Basu, A.; Ghatak, S. Physicochemical characteristics of alumina gel in hydroxyhydrogel and normal form. *Ceram. Int.* **2005**, *31*, 831–838.
36. Wilson, S. Phase transformations and development of microstructure in boehmite-derived transition aluminas. *Proc. Brit. Ceram. Soc.* **1979**, *28*, 281–294.
37. Igor Levin, D.B. Metastable alumina polymorphs crystal structures and transition sequences. *J. Am. Ceram. Soc.* **1998**, *81*, 1995–2012.
38. Brindley, G.; Choe, J. The reaction series, gibbsite→chi alumina→kappa alumina→corundum. *Am. Mineral.* **1961**, *46*, 771–785.
39. Yan, F.; Huang, H. Habit evolution of alumina crystallite during κ- to α-phase transformation. *Chin. J. Process Eng.* **2004**, *4*, 366–370.
40. Chang, P.; Yen, F.; Cheng, K.; Wen, H. Examinations on the critical and primary crystallite sizes during θ- to α-phase transformation of ultrafine alumina powders. *Nano Lett.* **2001**, *1*, 253–261.
41. Bagwell, R.; Messing, G. Effect of seeding and water vapor on the nucleation and growth of γ-Al_2O_3 from α-Al_2O_3. *J. Am. Ceram. Soc.* **1999**, *82*, 825–832.
42. Arai, H.; Machida, M. Thermal stabilization of catalyst supports and their application to high-temperature catalytic. *Appl. Catal. A-Gen.* **1996**, *138*, 161–176.
43. Barth, C.; Reichling, M. Imaging the atomic arrangements on the high-temperature reconstructed α-Al_2O_3 (0001) surface. *Nature* **2001**, *414*, 54–57.
44. Mohri, M.; Uchida, Y.; Sawabe, Y.; Watanabe, H. α-Alumina. U.S. Patent 6165437, 26 December 2000.